Topological domain wall states in a nonsymmorphic chiral chain

Wojciech Brzezicki [ORCID] and Timo Hyart

International Research Centre MagTop, Institute of Physics, Polish Academy of Sciences,
Aleja Lotnikow 32/46, PL-02668 Warsaw, Poland

The Su-Schrieffer-Heeger (SSH) model, containing dimerized hopping and a constant onsite energy, has become a paradigmatic model for one-dimensional topological phases, soliton excitations, and fractionalized charge in the presence of chiral symmetry. Motivated by the recent developments in engineering artificial lattices, we study an alternative model where hopping is constant but the onsite energy is dimerized. We find that it has a nonsymmorphic chiral symmetry and supports topologically distinct phases described by a $\mathbb{Z}_2$ invariant ν. In the case of multimode ribbon we also find topological phases protected by hidden symmetries and we uncover the corresponding $\mathbb{Z}_2$ invariants ν_n. We show that, in contrast to the SSH case, zero-energy states do not necessarily appear at the boundary between topologically distinct phases, but instead these systems support a new kind of bulk-boundary correspondence: The energy of the topological domain wall states typically scales to zero as $1/w$, where w is the width of the domain wall separating phases with different topology. Moreover, under specific circumstances we also find a faster scaling $e^{-w/\xi}$, where ξ is an intrinsic length scale. We show that the spectral flow of these states and the charge of the domain walls are different than in the case of the SSH model.

The Su-Schrieffer-Heeger (SSH) model was originally introduced to describe the properties of conducting polymers, where the spontaneous symmetry breaking leads to dimerization of the sites along the chain [1–3]. Due to twofold degeneracy of the ground state a new type of excitation, a domain wall (DW) between different bonding structures, can exist. For the conducting polymers the width of the DW excitations is large and they can propagate along the chain. Thus, they can be considered as solitons in analogy to the shape-preserving propagating solutions of the nonlinear differential equations [3]. Moreover, the solitons in the SSH model have a remarkable effect on the electronic spectrum leading to an appearance of a bound state in the middle of the energy gap. This midgap state is understood as a topologically protected boundary mode and the SSH model serves as a paradigmatic example of chiral symmetric topological insulator [4,5]. Namely, the chiral symmetry allows us to block-off diagonalize the Hamiltonian and the winding of the determinant z_k of the off-diagonal block around the origin as a function k determines a topological invariant (see Fig. 1). Because this invariant is different on two sides of the DW, each DW carries zero-energy bound state. The DWs come in pairs so that the spectral flow is symmetric around zero energy and each DW carries a charge $q = \pm 1/2$ in analogy to the fractionally charged excitations studied in the quantum field theory [6]. This can be also understood in terms of modern notions of bulk obstructions and filling anomalies [7].

The idea of soliton excitations reappears in the context of 1D diatomic polymers in a form of the Rice-Mele model [8–10], which has been studied also in contexts of ferroelectricity [11,12] and organic salts [13,14]. In this model not only bond length alternates but also the onsite energy (mass) takes opposite sign for the even/odd lattice sites (Fig. 1). A very interesting feature of such a model is that its solitons can carry irrational charge $q = \frac{1}{2}(1 \pm f)$ [8], where f describes the breaking of the chiral symmetry [15]. The interest for these models has revived because they can be engineered in photonic systems [16,17], optical lattices [18–23], and nanostructures [24–29] in a controlled way, and in these systems also their emergence from spontaneous symmetry breaking [30] and the properties of the solitons can be tuned using external parameters [31–36]. Motivated by the new possibilities opened by these recent developments we focus on a special case of the Rice-Mele model where all the hopping amplitudes are equal and only the mass term alternates. We show that in this case the model has an interesting nonsymmorphic (NS) chiral symmetry and it supports a topologically nontrivial phase described by a nonsymmorphic chiral $\mathbb{Z}_2$ invariant ν. This invariant was found by Shiozaki, Sato, and Gomi in their pioneering work on nonsymmorphic topological insulators [37] and therefore we name the special case of the Rice-Mele model as the Shiozaki-Sato-Gomi (SSG) model. The peculiar property of the SSG model is that the bulk topological invariant does not guarantee the existence of the end states in an open system, because the boundary always breaks the NS chiral symmetry [37].

In this paper we analytically derive exact phase diagrams of SSG nanoribbons of arbitrary width and uncover hidden symmetries relying on interchange of transverse and longitudinal modes. In addition to the NS chiral $\mathbb{Z}_2$ invariant ν the multimode ribbons support $\mathbb{Z}_2$ invariants ν_n protected by the hidden symmetries. These invariants lead to a new kind of bulk-boundary correspondence: The energy of the topological domain wall states typically scales to zero as $1/w$, where w is the width of the domain wall separating phases with different topology. Moreover, under specific circumstances we also find a faster scaling $e^{-w/\xi}$, where ξ is an intrinsic length scale (Figs. 2, 4, and 5). The NS chiral symmetry in SSG model
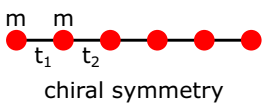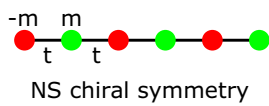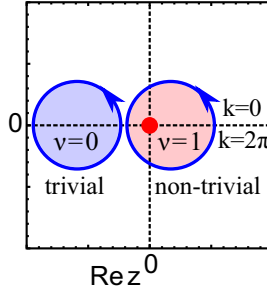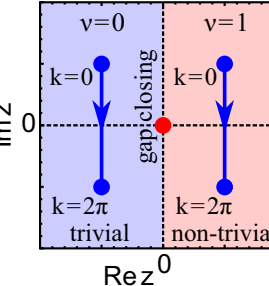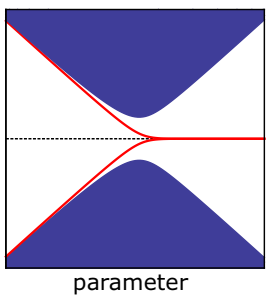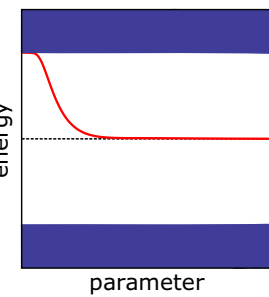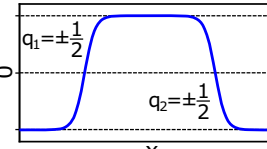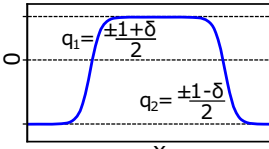
FIG. 1. Comparison of SSH and SSG models. The topological invariants are determined by the trajectory of the determinant z_k of the off-diagonal block of the Hamiltonian as a function k and the DWs separating topologically distinct phases lead to bound states, but in SSG model the bound state energy depends on the DW width, and the spectral flow and charge of the DW are different than in the SSH model.

FIG. 2. (a) Schematic view of the multimode SSG model. (b) Domain wall separating different mass m regions with different NS chiral $\mathbb{Z}_2$ invariants ν or hidden $\mathbb{Z}_2$ invariants ν_n. (c) Spectral flow of the DW states for multimode SSG chain as a function of the DW width w for $L_y = 7$, $L_x = 1000$, and $t_y = t_x$. DW separates regions with masses $m_1 = 0.2t_x$, $m_2 = -20t_x$, and $t_d = 0.6t_x$ differing only by ν. There is a single DW state whose energy approaches zero $\propto 1/w$. (d) The same for DW separating regions differing both by ν and ν_n with $m_1 = 0.25t_x$, $m_2 = -10t_x$, and $t_d = 0.05t_x$. In addition to the unpaired DW state with energy approaching zero $\propto 1/w$, there are hidden-symmetry protected DW states with energies approaching zero $\propto e^{-w/\xi}$, where ξ is an intrinsic length scale.

leads to several important differences in comparison to the SSH model (Fig. 1): (i) In SSH model the topological zero-energy end or DW states come in pairs and have zero energy for any DW width, whereas the SSG model supports unpaired DW states approaching zero energy with increasing w. Note that here we consider finite chains with open boundary conditions and the chains are made out of integer number of unit cells. An infinite SSH chain could also have an unpaired DW state but in the finite system the end states always guarantee
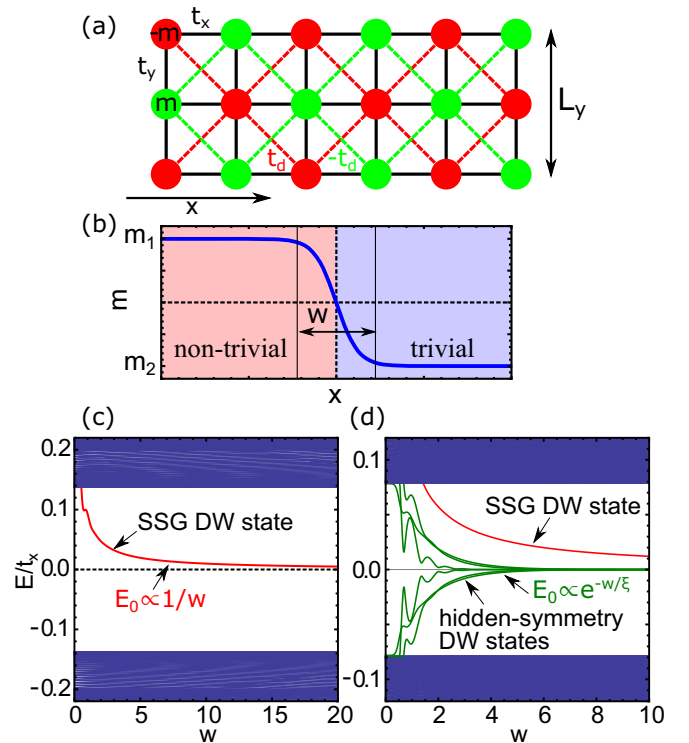
the the zero-energy states come in pairs. The SSG model is different because even in this kind of situation we can obtain a single zero-energy state at the smooth domain wall but there are no low-energy states at the sharp interface with vacuum. (ii) In the SSH model the charge of the DWs is $q = \pm\frac{1}{2}$, whereas for the SSG model we get irrational charges $q = \frac{\pm 1 - \delta}{2}, \frac{\pm 1 + \delta}{2}$ for solitons and antisolitons depending on whether the zero-energy state is occupied or empty. The DWs in the SSG model separate regions with different onsite energies $\pm m_1$ and $\pm m_2$ (mass terms) in the two sublattices (see Figs. 1 and 2), and $\delta = \frac{1}{2}(\zeta_2 - \zeta_1)$, where ζ_i is the difference of the bulk filling factors of the two sublattices in the region with mass m_i.

The k-space SSG Hamiltonian for a multimode wire is

$$\mathcal{H}_k = -m\sigma_z\tau_z + 2t_x \cos\frac{k}{2}\left(\cos\frac{k}{2}\sigma_x - \sin\frac{k}{2}\sigma_y\right)$$

$$+ t_y\tau_x + 2t_d \cos\frac{k}{2}\left(\sin\frac{k}{2}\sigma_x + \cos\frac{k}{2}\sigma_y\right)\tau_y, \quad (1)$$

where m is the mass, t_x and t_y are hopping amplitudes in the x and y directions, and t_d is the diagonal hopping amplitude

with opposite signs in the two sublattices [Fig. 2(a)]. Here σ_α are Pauli matrices describing the unit cell in the x direction, τ_α are $L_y \times L_y$ matrices describing transverse hopping $(\tau_x)_{pq} = \delta_{1,|p-q|}$, $(\tau_y)_{pq} = i\delta_{1,|p-q|}(-1)^p$, $(\tau_z)_{pq} = \delta_{pq}(-1)^p$, and L_y is the width in the y direction. For $L_y = 2$ operators τ_α are equivalent to σ_α and in the special case $L_y = 1$ we set $\tau_z = 1$ and $\tau_x = \tau_y = 0$. Because the SSG model belongs to symmetry class AI [5] (for list of symmetries see Appendix A) the only known topological invariant is the NS chiral $\mathbb{Z}_2$ invariant ν [37].

To calculate the topological invariant ν we rewrite the Hamiltonian in a block off-diagonal form in the eigenbasis of NS chiral operator $S_k = \sin\frac{k}{2}\sigma_x\tau_z + \cos\frac{k}{2}\sigma_y\tau_z$ that anticommutes with $\mathcal{H}_k$. The determinant z_k of the off-diagonal block is a complex number and its trajectory in the complex plane as a function k determines the topological invariant [37]. Namely, due to nonsymmorphicity of S_k the period of z_k is 4π and in a properly chosen basis it satisfies constraints $\mathrm{Im}z_k = -\mathrm{Im}z_{k+2\pi}$ and $\mathrm{Re}z_k = \mathrm{Re}z_{k+2\pi}$, so that the trajectory z_k starts at $k = 0$ and ends at $k = 2\pi$ with the same real part but with opposite imaginary part. Thus the parity of the number of times the trajectory z_k crosses the positive real semiaxis for $k \in [0, 2\pi]$ is a $\mathbb{Z}_2$ topological invariant because it cannot be changed without closing the gap or breaking the NS chiral symmetry (see Fig. 1). In our case the mirror symmetry $M_x = \cos\frac{k}{2} - i\sin\frac{k}{2}\sigma_z$ becomes identity in the eigenbasis of S_k (see Appendix A) so that $z_k = z_{-k}$. For this reason $\mathrm{Im}z_\pi = 0$ and the formula for the ν gets simplified to

$$\nu = \mathrm{sign}\,\mathrm{Re}z_\pi \qquad (2)$$

in analogy to the simplification of the invariant for topological insulators in the presence of inversion symmetry [38]. The band inversion corresponding to a change of ν happens at $k = \pi$ and $m = 0$. We find that

$$\nu = \begin{cases} \frac{1}{2}[1 + \mathrm{sign}(m)] & \text{if } L_y = 2n - 1 \\ 0, & \text{if } L_y = 2n \ (n \in \mathbb{N}_+) \end{cases}. \qquad (3)$$

In Fig. 3 we show the topological phase diagrams of the SSG model at $L_y = 6, 7$ as functions of m/t_x and t_d/t_x, setting $t_y = t_x$. Surprisingly we find more phases than predicted by the ν invariant. The gap closes not only for $m = 0$ at $k = \pi$ when L_y is odd but also for any L_y along lines $m = m_n$ at $k = k_n$, where

$$m_n = \frac{t_d t_y}{t_x}\varepsilon_n^2, \quad k_n = \pm 2\arccos\left[\frac{t_y}{2t_x}\varepsilon_n\right], \quad \varepsilon_n = 2\cos\frac{n\pi}{L_y+1} \qquad (4)$$

and $n = 1, 2, \ldots, \lfloor L_y/2 \rfloor$ provided that

$$\left|\frac{t_y}{2t_x}\varepsilon_n\right| \leqslant 1. \qquad (5)$$

This means that in the limit of very wide ribbon ($L_y \to \infty$) the phase diagram consists of a quasicontinuous set of lines $t_d = \gamma_n m$ with slopes γ_n ranging between $\frac{t_x}{4t_y}$ and ∞. The natural question to ask now is what is the origin of these gap-closing lines? The answer are the hidden symmetries, that can be found at the magical k_n points, yielding to new $\mathbb{Z}_2$ invariants ν_n.
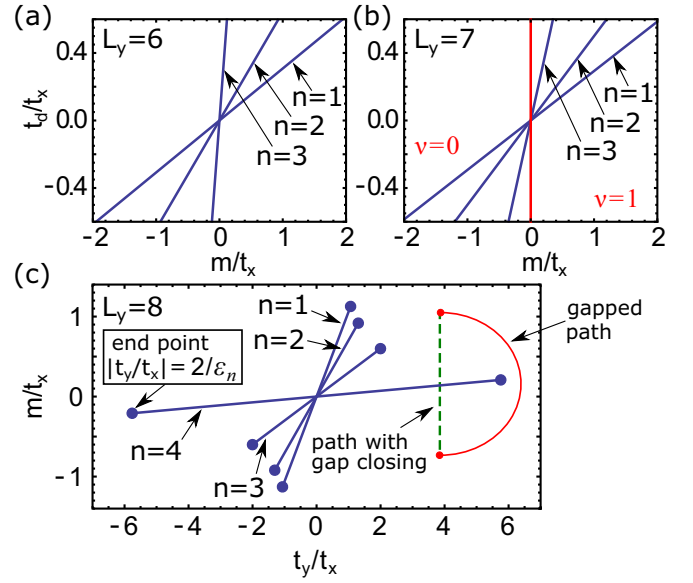

FIG. 3. (a), (b) Phase diagrams of the multimode SSG model in the m-t_d plane for $L_y = 6, 7$ and $t_y = t_x$. The phase transition line between different ν phases protected by the NS chiral symmetry is shown in red and phase transition lines between different ν_n protected by hidden symmetries are shown in blue. (c) Phase diagram in the $m - t_y$ plane for $L_y = 8$ and $t_d = 0.3t_x$. Each hidden symmetry $n = 1, 2, \ldots, \lfloor L_y/2 \rfloor$ exists only if condition (5) is satisfied. Therefore, it is possible to connect phases with different ν_n without closing the bulk gap by choosing a path in the parameter space which goes outside the region where the hidden symmetry exists.

To see the hidden symmetries we rotate σ_α matrices by angle $\frac{k}{2}$ around the z axis and use the eigenbasis of τ_x to transform the operators τ_α in a block-diagonal form, where the blocks are given by (see Appendix B)

$$\tau_{x,n} = \varepsilon_n\sigma'_x, \quad \tau_{y,n} = \varepsilon_n\sigma'_y, \quad \tau_{z,n} = \sigma'_z,$$

and σ'_α is a new set of Pauli matrices. For odd L_y the blocks $n = 0$ is given by $\tau_{x,0} = \tau_{y,0} = 0$ and $\tau_{z,0} = 1$. After this transformation the Hamiltonian (1) also has a block-diagonal form

$$\mathcal{H}'_{k,n} = -m\sigma_z\sigma'_z + 2t_x\cos\frac{k}{2}\sigma_x$$
$$+ 2t_d\varepsilon_n\cos\frac{k}{2}\sigma_y\sigma'_y + t_y\varepsilon_n\sigma'_x. \qquad (6)$$

Now we notice that $\mathcal{H}'_{k,n}$ is invariant under interchange of σ and σ' operators if $2t_x\cos\frac{k}{2} = t_y\varepsilon_n$ which provides the condition for gap closing points in the k space [Eq. (4)]. The spin-interchange $X_{12}\vec{\sigma}X_{12} = \vec{\sigma}'$ and vice versa is realized by operator $X_{12} = \frac{1}{2}(1 + \vec{\sigma}\cdot\vec{\sigma}')$ [39]. The spectrum of X_{12} consists of single -1 (singlet state) and three $+1$ (triplet states) eigenvalues. Thus $\mathcal{H}'_{k,n}$ in the eigenbasis of X_{12} becomes block diagonal with one block being 1×1 and the other being 3×3. Therefore we can define a topological $\mathbb{Z}_2$ invariant based on the sign of the matrix element of the 1×1 block. It changes at the gap closing lines defined by Eq. (4) so that it takes the form

$$\nu_n = \frac{1}{2}\{1 + \mathrm{sign}\,[m - m_n]\}. \qquad (7)$$

We conclude that the full topological description the SSG model is given by a vector $\{\nu, \nu_1, \nu_2, \ldots, \nu_{\lfloor L_y/2 \rfloor}\}$ because changes of these invariants coincide with all the gap closing lines in the phase diagram. Each hidden symmetry $n = 1, 2, \ldots, \lfloor L_y/2 \rfloor$ exists only if condition (5) is satisfied. Therefore, it is possible to connect phases with different ν_n without closing the bulk gap by choosing a path in the parameter space which goes outside the region where the hidden symmetry exists [see Fig. 3(c)], distinguishing the hidden-symmetric topological phases from the ones protected by structural symmetries. Note that in the two-dimensional limit where $t_x = t_y$ and the system is periodic in both directions the hidden symmetries become a mirror symmetry with respect to the $\hat{x} + \hat{y}$ line, but the hidden symmetries can exist even if the mirror symmetry is absent (see Appendix C).

After establishing topological properties of the SSG ribbon we now turn our attention to the bulk-boundary correspondence. In Ref. [37] it was argued that a NS chiral $\mathbb{Z}_2$ invariant does not generically support end states in one dimension because the boundary necessarily breaks the S_k symmetry. This however does not exclude a special type of smooth DWs from having zero energy bound states. To obtain analytical insights we can develop a continuum model for odd L_y by expanding $\mathcal{H}_k$ around the gap closing point at $k = \pi$ and get

$$\mathcal{H}_{\text{eff}} = v\delta k\sigma_x - m\sigma_y \quad (v > 0). \tag{8}$$

Now we create a DW of width w in the real space

$$m(x) = \frac{m_2 + m_1}{2} + \frac{m_2 - m_1}{2} \tanh \frac{x}{w} \tag{9}$$

between regions with positive mass $m_1 = m_0$ and negative mass $m_2 = -m_0$ ($m_0 > 0$), separating phases with $\nu = 1$ and $\nu = 0$ [Figs. 2(b) and 4(a)], and we find that a zero-energy eigenstate of $\mathcal{H}_{\text{eff}}$ exists in a form

$$\psi(x) = \left[0 \left(\cosh \frac{x}{w}\right)^{-m_0 w/v}\right]^T / \mathcal{N}, \tag{10}$$

where $\mathcal{N}$ is a normalization factor. This however does not take into account the fact that the chiral symmetry of $\mathcal{H}_{\text{eff}}$ becomes NS if one goes beyond linear order in δk. Therefore, we implemented numerically such a DW, for which $|m|$ is constant within a unit cell as follows from Eq. (8), and calculated the energy of the DW state as a function of w [Figs. 2(c), 2(d), and 4(a)]. This way we find that the energy of the topological DW state approaches zero as $1/w$ whereas the energies of the other bound states scale as $1/\sqrt{w}$. This means that the topological DW state can be distinguished from other bound states based on the scaling behavior because its energy approaches zero faster than the energies of the other states. We emphasize that the scaling of the energy to zero as $1/w$ or faster is a robust property of these topological DW states. In the continuum model this state would have zero energy and the lattice effects can give maximally a correction proportional to $1/w$. The robustness against perturbations preserving the NS chiral symmetry is demonstrated in Appendix D. On the other hand, in Appendix E we show that the DW state is exponentially localized around the center of the DW, i.e., such position $x = x_0$ that $m(x_0) = 0$, and the localization length decreases with increasing w, as one could expect. The $1/\sqrt{w}$
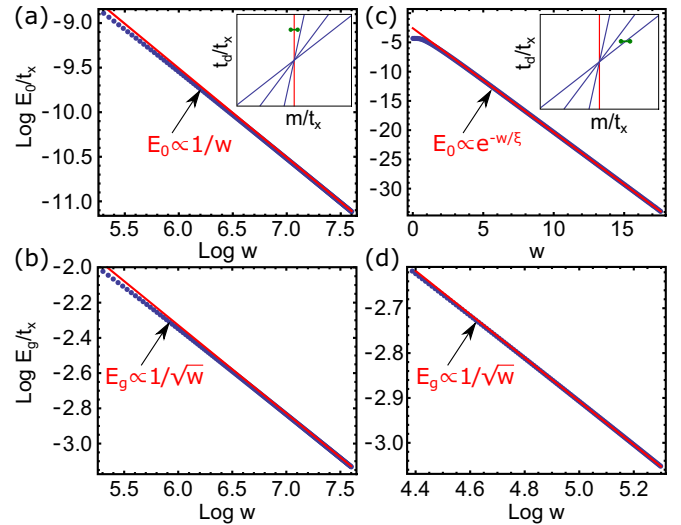

FIG. 4. Scaling of the energy of the topological DW state E_0 and the lowest energy of the nontopological states E_g for a multimode SSG model as a function of the DW width w. (a), (b) DW between phases with $m_1 = 0.12t_x$ and $m_2 = -0.12t_x$ distinguished by NS chiral invariant ν. Here we have chosen $t_d = 0.4t_x$. (c), (d) DW between phases with $m_1 = 0.7t_x$ and $m_2 = 0.1t_x$ distinguished by the hidden symmetry protected invariant ν_n. Here we have chosen $t_d = 0.25t_x$. Insets show the phases which are separated by the DWs. The other parameters are $t_y = t_x$, $L_y = 7$, and $L_x = 10\,000$.

scaling of the bulk gap can be understood as well. By inserting an expansion $m(x) \simeq m_0 \frac{x}{w}$ around $x = 0$ to Hamiltonian $\mathcal{H}_{\text{eff}}$ and eliminating ψ_1 we obtain a Harmonic oscillator equation for ψ_2

$$-v^2\psi_2''(x) + \frac{m_0^2}{w^2}x^2\psi_2(x) = \left(E^2 + \frac{m_0 v}{w}\right)\psi_2(x). \tag{11}$$

The energies of this problem are given by

$$E_n = \sqrt{\frac{2nm_0 v}{w}}, \quad n = 0, 1, 2, \ldots. \tag{12}$$

The $n = 0$ solution gives the topological DW state and the energies of the other states scale as $1/\sqrt{w}$. We have just shown that the in-gap state at the DW between two topologically distinct domains follows from the continuum-limit model and adiabatic evolution of the states when DW is sufficiently smooth. This is quite a different case to the one discussed in [40] where a surface state also appears in the presence of a NS symmetry but it also requires a surface potential.

We find even more striking bulk-boundary correspondence for phases described by ν_n invariants. In Figs. 2(d), 4(c), and 4(d) we show the scaling of energies of the topological DW states and the nontopological states as a function of w when the masses m_1 and m_2 are chosen so that the DW separates two different ν_n phases. The energies of the nontopological states behave in the same way as before, scaling as $1/\sqrt{w}$, but the energies of the hidden-symmetry protected topological DW states scale as $e^{-w/\xi}$. By expanding Hamiltonian around
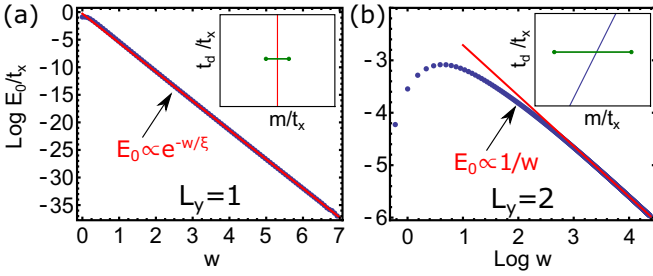
FIG. 5. Dependence of the scaling of the energy E_0 on the microscopic details of the DW. (a) E_0 for a DW between phases distinguished by ν invariant can show exponential scaling if the masses in the two sublattices vary as $\tanh \frac{2i-1}{2w}$ and $-\tanh \frac{2i}{2w}$, where i is a position of the unit cell along the chain. Notice that in our default DWs, where the $1/w$ scaling is obtained, the mass terms are given by $\pm \tanh \frac{i}{w}$. The other parameters are $m_{1,2} = \pm t_x$ and $L_y = 1$. (b) E_0 for a DW between phases distinguished by ν_n invariant can show $1/w$ scaling if the masses vary as $\pm \tanh \frac{i+j}{w}$, where j labels the chains stacked in the y direction. The other parameters are $t_y = t_x$, $L_x = 10\,000$.

the gap closing points $\pm k_n$ we get two similar bound state solutions as for $k = \pi$. However, these solutions do not give zero-energy states even in the continuum model because the gap closes at two different momenta so that these bound states hybridize leading to nonzero energy. Nevertheless, in Appendix G we show using the properties of the Schwartz functions that in the continuum model their overlap vanishes exponentially fast with w which allows the possibility of the exponential scaling. Nevertheless, the lattice effects could lead to $1/w$ corrections also in this case. Therefore, we have studied more carefully how the scaling of the energies depends on the details of the DW. We find that for a specific type of DW it is possible to obtain an exponential decay of energy $e^{-w/\xi}$ also in the case of the DWs separating different ν phases, and conversely it is possible to obtain $1/w$ scaling for a DW separating different ν_n phases (see Fig. 5). In this way, by manipulating the details of the DWs, we are able to see that the behavior of both types of DW states are equivalent. This leads to a robust conclusion that the energies of the DW states scale as $1/w$ or faster. While the $1/w$ scaling is expected to be generic based on the analytical arguments given above, the faster exponential scaling, which we numerically find in some specific circumstances, means that the $1/w$ corrections are not always present. The analytical model-independent theoretical understanding of the conditions for the exponential scaling is an interesting direction for future research. By setting m_1 and m_2 is such a way that all the gap closing lines are crossed on the way from m_1 to m_2 we can always obtain an extensive number of DW states L_y both for even and odd L_y.

An interesting property of the SSG model is that when the width of the DW w increases a single state separates from the bulk spectrum and tends to zero from above or below [Fig. 2(c)]. This asymmetric spectral flow needs to be taken into account when calculating the charges for solitons and antisolitons (see Appendix H). For $L_y = 1$ we obtain $q_0 = \frac{\pm 1 - \delta}{2}, \frac{\pm 1 + \delta}{2}$ for solitons and antisolitons depending on whether the zero-energy state is occupied or empty.

Here $\delta = \frac{\zeta_2 - \zeta_1}{2}$,

$$\zeta_i = \frac{2}{\pi} \frac{m_i}{\sqrt{m_i^2 + 4t_x^2}} K\left(\frac{4t_x^2}{m_i^2 + 4t_x^2} \right)$$

are the differences of the bulk filling factors of the two sublattices in the region with mass $m_1 > 0$ and $m_2 < 0$, and $K(x)$ is the complete elliptic integral of the first kind. The DWs between different hidden-symmetric topological phases carry charges $q_n = 0, \pm 1$, so that for a general DW the charge is the sum of q_0 and the charges q_n contributed by the transverse modes supporting transitions between different hidden-symmetric topological phases.

To summarize, we have analytically described the topological properties of the SSG model and propose it as a paradigmatic model for NS chiral-symmetric topological phases. We have shown that a smooth DW supports zero energy state(s) if the DW separates regions with different NS chiral invariant ν or different hidden-symmetry invariants ν_n. In addition to engineered artificial lattices [16,18–24,26–29] our findings are also relevant in the context of low-dimensional binary compounds supporting surface atomic steps. In these systems the surface steps lead to one-dimensional topological modes and the system obeys NS chiral symmetry, so that DWs between topologically distinct phases can support DW states [41], providing a possible explanation for the zero-bias conductance peak observed in the recent experiment [42].

APPENDIX A: HAMILTONIAN AND ITS SYMMETRIES

The SSG Hamiltonian on a square lattice has a form

$$\mathcal{H} = t_x \sum_{\vec{j}} (c_{\vec{j}}^\dagger c_{\vec{j}+\hat{x}} + \text{H.c.}) + t_y \sum_{\vec{j}} (c_{\vec{j}}^\dagger c_{\vec{j}+\hat{y}} + \text{H.c.})$$
$$+ t_d \sum_{s=\pm 1} \sum_{\vec{j}} (-1)^{j_x+j_y+1} (c_{\vec{j}}^\dagger c_{\vec{j}+\hat{x}+s\hat{y}} + \text{H.c.})$$
$$+ m \sum_{\vec{j}} (-1)^{j_x+j_y+1} c_{\vec{j}}^\dagger c_{\vec{j}}, \tag{A1}$$

where m is the mass term, t_x and t_y are hopping amplitudes along the x and y directions, and t_d is the diagonal hopping amplitude. The k-space form is given by

$$\mathcal{H}_k = -m\sigma_z\tau_z + 2t_x \cos\frac{k}{2}\left(\cos\frac{k}{2}\sigma_x - \sin\frac{k}{2}\sigma_y \right)$$
$$+ t_y\tau_x + 2t_d \cos\frac{k}{2}\left(\sin\frac{k}{2}\sigma_x + \cos\frac{k}{2}\sigma_y \right)\tau_y, \tag{A2}$$

where τ_α operators are given by matrices

$$
\tau_x = \begin{pmatrix} 0 & 1 & 0 & 0 & \cdots \\ 1 & 0 & 1 & 0 & \cdots \\ 0 & 1 & 0 & 1 & \\ 0 & 0 & 1 & 0 & \\ \vdots & \vdots & & & \ddots \end{pmatrix},
$$

$$
\tau_y = \begin{pmatrix} 0 & -i & 0 & 0 & \cdots \\ i & 0 & i & 0 & \cdots \\ 0 & -i & 0 & -i & \\ 0 & 0 & i & 0 & \\ \vdots & \vdots & & & \ddots \end{pmatrix}, \qquad (A3)
$$

and

$$
\tau_z = \begin{pmatrix} 1 & 0 & 0 & 0 & \cdots \\ 0 & -1 & 0 & 0 & \cdots \\ 0 & 0 & 1 & 0 & \\ 0 & 0 & 0 & -1 & \\ \vdots & \vdots & & & \ddots \end{pmatrix},
$$

$$
\tau_a = \begin{pmatrix} \cdots & 0 & 0 & 0 & 1 \\ \cdots & 0 & 0 & 1 & 0 \\ & 0 & 1 & 0 & 0 \\ & 1 & 0 & 0 & 0 \\ \iddots & & & \vdots & \vdots \end{pmatrix}. \qquad (A4)
$$

Here we defined additional matrix τ_a which is needed to construct some of the symmetry operators.

Depending on system width L_y being even or odd the system has different symmetry properties. However, some symmetries are common for both cases. The one which is most relevant here is the nonsymmorphic (NS) chiral symmetry defined as $S_k = \sin\frac{k}{2}\sigma_x\tau_z + \cos\frac{k}{2}\sigma_y\tau_z$ which satisfies $S_k\mathcal{H}_k S_k^{-1} = -\mathcal{H}_k$. The k dependence in S_k is intrinsic and follows from the half lattice translation that is needed to go from one sublattice to the other. We also have a time-reversal symmetry for spinless particles $\mathcal{T}\mathcal{H}_k\mathcal{T}^{-1} = \mathcal{H}_{-k}$, where $\mathcal{T} = \mathcal{K}$ is complex conjugation. Finally, for any L_y we have a symmetry with respect to a mirror line perpendicular to the x direction, passing through a lattice site, taking a form of $M_x = \cos\frac{k}{2} - i\sin\frac{k}{2}\sigma_z$ and acting as $M_x\mathcal{H}_k M_x^{-1} = \mathcal{H}_{-k}$. Despite the k dependence this is a symmorphic symmetry. By shifting a mirror line to cut a middle of a bond we can also get a chiral mirror symmetry $\overline{M}_x = \sigma_y\tau_z$ yielding relation $\overline{M}_x\mathcal{H}_k\overline{M}_x^{-1} = -\mathcal{H}_{-k}$.

For odd L_y we have another mirror symmetry with respect to a line perpendicular to the y direction $M_y\mathcal{H}_k M_y^{-1} = \mathcal{H}_k$, where $M_y = \tau_a$. For even L_y mirror M_y does not exist but we have a particle-hole symmetry $\mathcal{C} = i\mathcal{K}\sigma_z\tau_a\tau_z$ and inversion symmetry $I = \sigma_x\tau_a$, yielding relations $\mathcal{C}\mathcal{H}_k\mathcal{C}^{-1} = -\mathcal{H}_{-k}$ and $I\mathcal{H}_k I^{-1} = \mathcal{H}_{-k}$.

It is important to notice that in the eigenbasis of S_k the mirror symmetry operator M_x operator transforms to identity. This is possible because if we put eigenvectors of S_k in the columns of unitary matrix $\mathcal{U}_k$ then M_x is transformed as $\tilde{M}_x = \mathcal{U}_{-k}^\dagger M_x\mathcal{U}_k$. Note that this is not similarity transformation so the spectrum of M_x is not left invariant. The form of transformation is dictated by the mirror-symmetry relation with the

Hamiltonian in the new basis. Denoting $\tilde{\mathcal{H}}_k = \mathcal{U}_k^\dagger M_x\mathcal{U}_k$ we get that $\tilde{M}_x\tilde{\mathcal{H}}_k\tilde{M}_x^{-1} = \tilde{\mathcal{H}}_{-k}$.

APPENDIX B: HIDDEN SYMMETRIES

To see the hidden symmetries we first transform $\mathcal{H}_k$ to $\mathcal{H}_k' = R_{k/2}^\dagger\mathcal{H}_k R_{k/2}$ using $R_{k/2} = \exp(i\frac{k}{4}\sigma_z)$ to get

$$
\mathcal{H}_k' = -m\sigma_z\tau_z + 2t_x\cos\frac{k}{2}\sigma_x + 2t_d\cos\frac{k}{2}\sigma_y\tau_y + t_y\tau_x. \quad (B1)
$$

The eigenfunctions of τ_x corresponding to eigenvalues ε_n are $\psi_n(j) = \sqrt{\frac{2}{L_y+1}}\sin\frac{nj\pi}{L_y+1}$, where j labels sites in the y direction and n labels modes ($j, n = 1, 2, \ldots, L_y$). We can use these transverse modes to construct a new basis $|\phi_{2n-1}\rangle = (|\psi_n\rangle + |\psi_{L_y+1-n}\rangle)/\sqrt{2}$ and $|\phi_{2n}\rangle = (|\psi_n\rangle - |\psi_{L_y+1-n}\rangle)/\sqrt{2}$ for $n = 1, 2, \ldots, \lfloor L_y/2\rfloor$ and if L_y is odd $|\phi_0\rangle = |\psi_{\lceil L_y/2\rceil}\rangle$. In this basis τ_x, τ_y, and τ_z have block-diagonal forms with $\lfloor L_y/2\rfloor$ diagonal blocks given by

$$
\tau_{x,n} = \varepsilon_n\sigma_x', \quad \tau_{y,n} = \varepsilon_n\sigma_y', \quad \tau_{z,n} = \sigma_z',
$$

where σ_α' is a new set of Pauli matrices, and for odd L_y the block $n = 0$ is given by $\tau_{x,0} = \tau_{y,0} = 0$ and $\tau_{z,0} = 1$. Thus the Hamiltonian has a block-diagonal form

$$
\mathcal{H}_{k,n}' = -m\sigma_z\sigma_z' + 2t_x\cos\frac{k}{2}\sigma_x + 2t_d\varepsilon_n\cos\frac{k}{2}\sigma_y\sigma_y' + t_y\varepsilon_n\sigma_x'
$$
(B2)

supporting the hidden symmetries discussed in the main text.

APPENDIX C: HIDDEN SYMMETRIES IN A TWO-DIMENSIONAL LIMIT

In the case when the system is periodic both in the x and y direction it can be described by a k-space Hamiltonian written in a form of

$$
\mathcal{H}_{\vec{k}} = -m\sigma_z\tau_z + 2t_x\cos\frac{k_x}{2}\left(\cos\frac{k_x}{2}\sigma_x - \sin\frac{k_x}{2}\sigma_y\right)
$$
$$
+ 2t_y\cos\frac{k_y}{2}\left(\cos\frac{k_y}{2}\tau_x - \sin\frac{k_y}{2}\tau_y\right)
$$
$$
+ 4t_d\cos\frac{k_x}{2}\cos\frac{k_y}{2}\left(\sin\frac{k_x}{2}\sigma_x + \cos\frac{k_x}{2}\sigma_y\right)
$$
$$
\times\left(\sin\frac{k_y}{2}\tau_x + \cos\frac{k_y}{2}\tau_y\right), \quad (C1)
$$

where σ_α and τ_α are the Pauli matrices describing the unit cell along x and y directions. Similarly as before, to see the hidden symmetries we transform $\mathcal{H}_{\vec{k}}$ to $\mathcal{H}_{\vec{k}}' = R_{\vec{k}}^\dagger\mathcal{H}_{\vec{k}}R_{\vec{k}}$ using $R_{\vec{k}} = \exp(\frac{i}{4}[k_x\sigma_z + k_y\tau_z])$ to get

$$
\mathcal{H}_{\vec{k}}' = -m\sigma_z\tau_z + 2t_x\cos\frac{k_x}{2}\sigma_x + 2t_y\cos\frac{k_y}{2}\tau_x
$$
$$
+ 4t_d\cos\frac{k_x}{2}\cos\frac{k_y}{2}\sigma_y\tau_y. \quad (C2)
$$

Obviously $\mathcal{H}_{\vec{k}}'$ (and already $\mathcal{H}_{\vec{k}}$) is invariant under interchange of σ and τ operators if

$$
t_x\cos\frac{k_x}{2} = t_y\cos\frac{k_y}{2}. \quad (C3)
$$

The spin-interchange $X_{12}\vec{\sigma} X_{12} = \vec{\sigma}'$ and vice versa is realized by operator $X_{12} = \frac{1}{2}(1 + \vec{\sigma} \cdot \vec{\tau})$. Coming back to the original basis of Eq. (C1) we find that X_{12} operator gives rise to two different symmetry operations,

$$M_{xy} \equiv R_{k_y, k_x} X_{12} R^\dagger_{k_x, k_y} = \frac{1}{2}(1 + \vec{\sigma} \cdot \vec{\tau}), \qquad (C4)$$

$$\mathcal{X}_{\vec{k}} \equiv R_{k_x, k_y} X_{12} R^\dagger_{k_x, k_y} = \frac{1}{2}\left(1 + \cos\frac{k_x - k_y}{2}[\sigma_x\tau_x + \sigma_y\tau_y]\right.$$
$$\left. + \sin\frac{k_x - k_y}{2}[\sigma_x\tau_y - \sigma_y\tau_x] + \sigma_z\tau_z\right). \qquad (C5)$$

The first one is the mirror symmetry with respect to the $\hat{x} + \hat{y}$ line. One can verify that if $t_x = t_y$ then

$$M_{xy}\mathcal{H}_{k_x, k_y}M_{xy}^{-1} = \mathcal{H}_{k_y, k_x}. \qquad (C6)$$

Therefore M_{xy} commutes with $\mathcal{H}_{\vec{k}}$ for $k_x = k_y$. Note that this also holds for a finite periodic system where $L_x \neq L_y$, when the discretized quasimomentum satisfies $k_x = k_y$. On the other hand, the hidden symmetry operator $\mathcal{X}_{\vec{k}}$ satisfies

$$\mathcal{X}_{k_x, f(k_x)}\mathcal{H}_{k_x, f(k_x)}\mathcal{X}_{k_x, f(k_x)}^{-1} = \mathcal{H}_{k_x, f(k_x)}, \qquad (C7)$$

as long as condition (C3) holds which means that

$$k_y = f(k_x) = 2\arccos\left(\frac{t_x}{t_y}\cos\frac{k_x}{2}\right). \qquad (C8)$$

Note that this does not require that $t_x = t_y$. Hence, the hidden symmetry is a different operator than the mirror symmetry M_{xy} even though it originates from the same X_{12} operator in the $R_{\vec{k}}$-transformed basis. It can be regarded as an interchange of longitudinal and transverse modes in the system. Note that condition (C3) trivially generalizes to the condition found for a multimode wire.

APPENDIX D: ROBUSTNESS OF THE DW STATES

To check whether the DW states protected by the NS chiral symmetry are indeed topologically protected we consider a single-mode SSG wire. An arbitrary perturbation that preserve the NS chiral symmetry $\mathcal{S}_k$ has a form of

$$\mathcal{V}_k = a_k\sigma_z + b_k\left(\cos\frac{k}{2}\sigma_x - \sin\frac{k}{2}\sigma_y\right), \qquad (D1)$$

where k-dependent coefficients should have such form that $\mathcal{V}_k$ is 2π periodic in k. Hence we have

$$a_k = p_0 + \sum_{i=1}^r (p_{2i-1}\sin(ik) + p_{2i}\cos(ik)),$$

$$b_k = \sum_{i=1}^r \left(q_{2i-1}\sin\frac{(2i-1)k}{2} + q_{2i}\cos\frac{(2i-1)k}{2}\right), \qquad (D2)$$

where r is the range of hoppings involved in $\mathcal{V}_k$.

In Fig. 6 we show the scaling of the energy of the DW state between two regions of opposite masses for a single-mode wire in the presence of perturbation $\mathcal{V}_k$. We choose $r = 10$ and we pick random p_n and q_n coefficients from the uniform distribution over the interval $[-0.1t_x, 0.1t_x]$. The masses are chosen as $m_{1,2} = \pm t_x$ so that such perturbation does not close the bulk gap. As we can see in Fig. 6(a) the energy E_0 of the
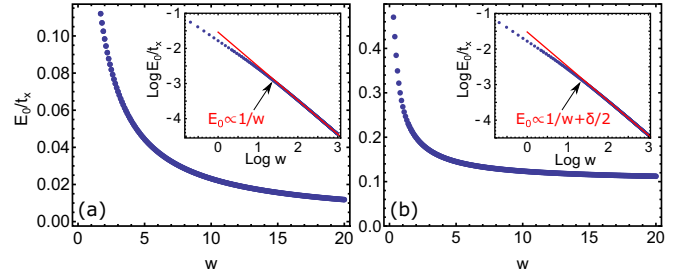

FIG. 6. Scaling of the energy of the topological DW state E_0 of a single-mode SSG model as a function of the DW width w in linear and logarithmic scales (insets). (a) We have added a generic perturbation that preserves NS chiral symmetry. (b) We have added a perturbation that breaks NS symmetry with $\delta = 0.1$. The parameters are $m_{1,2} = \pm t_x$ and $L_x = 10\,000$.

DW state still scales to zero as $1/w$. On the other hand, if we add a perturbation that breaks the NS chiral symmetry, for instance $\mathcal{V}_k = \delta\sigma_x$, the DW state should converge to a nonzero energy. In Fig. 6(b) we see that this is indeed the case for our single-mode wire E_0 scales like $1/w$ to δ.

APPENDIX E: LOCALIZATION OF THE DW STATES

In Fig. 7 we show the spectral flow and the local density of states for a DW state in a representative multimode chain with $L_y = 7$ for increasing width w of a domain wall between two domains with different NS $\mathbb{Z}_2$ invariant. We note that the DW state is exponentially localized around the center of the domain wall at $x = x_0$ [defined by $m(x_0) = 0$] and the localization length decreases with increasing w.

APPENDIX F: FERMI VELOCITY AT DIRAC POINTS $k = \pm k_n$

We notice that the Hamiltonian $\mathcal{H}'_{k,n}$ given by Eq. (B2) commutes with $\mathcal{P} = \sigma_x\sigma'_x$. The bands that cross at $k = \pm k_n$ can be found in the block $\mathcal{P} = -1$ of the Hamiltonian that
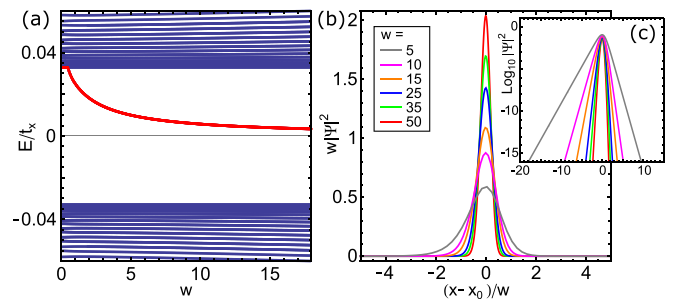

FIG. 7. (a) Spectral flow of the DW states for multimode SSG chain as function of the DW width w for $L_y = 7$, $L_x = 1000$, and $t_y = t_x$. DW separates regions with masses $m_1 = 0.2t_x$ and $m_2 = -0.4t_x$ and $t_d = 0.4t_x$. (b) Evolution of local density of states for the DW state for increasing w, x is the position along the chain (lines are continuously interpolated between the chain's sites as a guide for the eye) and x_0 is the center of the DW defined by $m(x_0) = 0$. Horizona axis is renormalized by w and vertical by $1/w$. (c) The linear-log version of plot (b).

takes the form,

$$\mathcal{H}'_{k,n,-} = -4\sin\frac{k+k_n}{4}\sin\frac{k-k_n}{4}(t_x\sigma_x + t_d\varepsilon_n\sigma_z)$$
$$- (m - m_n)\sigma_z. \tag{F1}$$

The remaining $\mathcal{P} = +1$ block is related by a shift of 2π in the k space and unitary transformation, namely $\mathcal{H}'_{k,n,+} = \sigma_z\mathcal{H}'_{k+2\pi,n,-}\sigma_z$. Consequently, the Fermi velocity at the Dirac points is given by

$$v_n = \pm t_x\sqrt{\left(1 - \frac{t_y^2}{4t_x^2}\varepsilon_n^2\right)\left(1 + \frac{t_d^2}{t_x^2}\varepsilon_n^2\right)}. \tag{F2}$$

APPENDIX G: OVERLAP OF TWO DOMAIN-WALL FUNCTIONS

We assume that the functional form of $m(x)$ is such that it only depends on parameter x/w. In analogy to the domain wall solution for a gap closing point at $k = \pi$ we get two solutions for $k = \pm k_n$ gap closings in a form (we ignore the spinor structure which would change as a function momentum and the normalization factor which is not important for the statements below)

$$\psi^{\pm}(x) = \exp\left[\pm ik_n x - v_n^{-1}\int_0^x m\left(\frac{x'}{w}\right)dx'\right]. \tag{G1}$$

Their overlap is

$$\langle\psi^-|\psi^+\rangle = \int_{-\infty}^{+\infty}\exp\left[2ik_n x - 2v_n^{-1}\int_0^x m\left(\frac{x'}{w}\right)dx'\right]dx \tag{G2}$$

and substituting $x = yw$ we get

$$\langle\psi^-|\psi^+\rangle = w\int_{-\infty}^{+\infty}\exp\left[2ik_n wy - 2wv_n^{-1}M(y)\right]dy, \tag{G3}$$

where $M(y) = \int_0^y m(y')dy'$. Assuming that $M(y) > 0$, $m(\infty) > 0$ and $m(-\infty) < 0$ as we expect from a domain wall, we notice that $f(y) = \exp\left[-2v_n^{-1}wM(y)\right]$ is a Schwartz function. This property does not depend on the details of the model (even if one goes beyond the linear order expansion in momentum) or the shape of the DW as long as the solutions $\psi_{\pm}$ are smooth functions decaying exponentially (or faster) far away from the DW. The Fourier transform of a Schwartz function is also a Schwartz function and therefore the overlap $\langle\psi^-|\psi^+\rangle$ must vanish quicker than any power of $1/(k_n w)$.

To see the exponential dependence explicitly we can assume for example $m(x/w) = m_0 x/w$. Then we obtain

$$\langle\psi^-|\psi^+\rangle = w\int_{-\infty}^{+\infty}\exp\left[2ik_n wy - wm_0 v_n^{-1}y^2\right]dy$$
$$= w\sqrt{\frac{\pi v_n}{wm_0}}\exp\left[-wk_n^2 v_n/m_0\right]. \tag{G4}$$

APPENDIX H: CHARGE OF A DOMAIN WALL

To understand the charge of the DW we start by calculating the charge appearing at the end of single-mode SSG chain

with open boundary conditions

$$\mathcal{H} = \begin{pmatrix} -m & t & 0 & 0 & \cdots \\ t & m & t & 0 & \cdots \\ 0 & t & -m & t & \cdots \\ 0 & 0 & t & m & \\ \vdots & \vdots & \vdots & & \ddots \end{pmatrix}. \tag{H1}$$

Assuming even number of sites $L = 2N$ the Hamiltonian can be Block diagonalized into 2×2 blocks similarly as in Appendix B, and the eigenstates can be found by diagonalizing these blocks. This way we find that the eigenenergies are $(n = 1, 2, \ldots, N)$

$$E_{n\pm} = \pm E_n, \ E_n = \sqrt{m^2 + 4t^2\cos^2\left(\frac{n\pi}{2N+1}\right)}. \tag{H2}$$

The eigenstate corresponding to E_{n-} at lattice site j is

$$\psi_{n,-}(j) = \frac{\sin\left(\frac{nj\pi}{2N+1}\right)}{\sqrt{2(2N+1)}}\left[[1 - (-1)^j]\sqrt{1 + \frac{m}{E_n}}\right.$$
$$\left. - [1 + (-1)^j]\sqrt{1 - \frac{m}{E_n}}\right]. \tag{H3}$$

The total end charge q_{end} at lattice sites $j = 1, \ldots, 2\xi$ (relative to the corresponding bulk charge ξ) is

$$q_{\text{end}} = \frac{2}{2N+1}\sum_{n=1}^{N}\sum_{j=1}^{2\xi}\sin^2\left(\frac{nj\pi}{2N+1}\right)\left[1 - (-1)^j\frac{m}{E_n}\right] - \xi$$
$$= \frac{1}{2N+1}\sum_{n=1}^{N}\sum_{j=1}^{2\xi}(-1)^j\cos\left(\frac{nj2\pi}{2N+1}\right)\frac{m}{E_n}$$
$$= -\frac{\zeta}{4} + \frac{1}{2}\frac{1}{2N+1}\sum_{n=1}^{N}\frac{\cos\left[(2\xi + \frac{1}{2})\frac{n2\pi}{2N+1}\right]}{\cos\left[\frac{1}{2}\frac{n2\pi}{2N+1}\right]}\frac{m}{E_n}$$
$$= \frac{\text{sign}(m) - \zeta}{4}, \tag{H4}$$

where

$$\zeta(m) = \frac{2}{2N+1}\sum_{n=1}^{N}\frac{m}{E_n} = \frac{2}{2\pi}\int_0^{\pi}dk\frac{m}{\sqrt{m^2 + 4t^2\cos^2(k/2)}}$$
$$= \frac{2}{\pi}\frac{m}{\sqrt{m^2 + 4t^2}}K\left(\frac{4t^2}{m^2 + 4t^2}\right) \tag{H5}$$

is the difference of the bulk filling factors of the two sublattices and

$$K(x) = \int_0^{\pi/2}d\theta\frac{1}{\sqrt{1 - x\sin^2(\theta)}} \tag{H6}$$

is the complete elliptic integral of the first kind. Here we have used

$$\frac{1}{4\pi}\int_0^\pi dk \frac{m\cos\left[(2\xi+\frac{1}{2})k\right]}{\sqrt{m^2+4t^2\cos^2\left(\frac{k}{2}\right)}\cos\left[\frac{1}{2}k\right]} = \frac{\text{sign}(m)}{4}, \quad (H7)$$

which is valid up to corrections which decay exponentially with increasing ξ. At the other end of the chain there is a charge $-q_{\text{end}}$.

Let's now consider a sharp DW between regions with mass m_i and m_j. If we first assume that we turn off the hopping connecting these two regions, we find that the region with mass m_i gives rise to the charge $-q_{\text{end},i}$ and the region with mass m_j gives rise to a charge $q_{\text{end},j}$ at the DW so that the total charge is

$$q_{\text{DW}} = \frac{\text{sign}(m_j)-\text{sign}(m_i)}{4} - \frac{\delta_{ji}}{2}, \quad (H8)$$

where we have defined

$$\delta_{ji} = \frac{\zeta(m_j)-\zeta(m_i)}{2}. \quad (H9)$$

This charge is exponentially localized at the DW and therefore when the hopping connecting the regions is turned on it causes only a local perturbation in the Hamiltonian (slightly redistributing the charge density locally) but does not influence the total charge localized at the DW. If both m_i and m_j have the same sign the regions are in the same topological phase and the $q_{\text{DW}} = -\delta_{ji}/2$. If the signs of the masses are different we have DW between two topologically distinct phases. We now consider two possible DWs: (i) Soliton where mass changes from $m_1 > 0$ to $m_2 < 0$ as a function of increasing x and (ii) antisoliton where mass changes from $m_2 < 0$ to $m_1 > 0$ as a function of increasing x (see Figs. 1 and 2 in the main text). We denote $\delta = \delta_{21}$.

(i) In the case of soliton the sharp DW carries a charge $q_{\text{DW}} = -(1+\delta)/2$. By increasing the width of the DW we find that the spectral flow is such that a state will approach zero energy from positive energies (see Fig. 2 in the main text). This means that if this zero-energy state is unoccupied the charge of the DW is q_{DW} and if it is occupied the charge is $q_{\text{DW}} + 1$. Thus we can summarize that the possible charges for soliton are

$$q_{\text{DW}} = \frac{\pm 1 - \delta}{2}. \quad (H10)$$

(ii) For antisoliton the charge of the sharp DW is $q_{\text{DW}} = (1+\delta)/2$. By increasing the width of the DW we find that the spectral flow is such that a state will approach zero energy from negative energies. This means that if this zero-energy state is unoccupied the charge of the DW is $q_{\text{DW}} - 1$ and if it is occupied the charge is q_{DW}. Thus we can summarize that the possible charges for antisoliton are

$$q_{\text{DW}} = \frac{\pm 1 + \delta}{2}. \quad (H11)$$

In the case of multimode SSG system we can separate the transverse modes n as discussed in Appendix B. We consider the cases (a) L_y even and (b) L_y odd separately.

(a) When L_y is even the Hamiltonian can be decomposed into 4×4 blocks given by Eq. (B2). Each of these blocks $n = 1, \ldots, L_y/2$ supports symmorphic chiral symmetries $C_{yz} = \sigma_y \sigma_z'$ and $C_{zy} = \sigma_z \sigma_y'$. Therefore using the argument given in Ref. [43] we find that each transverse mode n carries possible charges $q_n = -N_n/2, \ldots, N_n/2$, where N_n is the number of zero-energy states at the DW supported by transverse mode n and the value of charge q_n is determined by the number of occupied zero-energy states. In the case of smooth DWs each transverse mode supports $N_n = 2$ zero-energy states if ν_n is different on the two sides of the DW so that $q_n = -1, 0, 1$ (with two possible states corresponding to $q_n = 0$). If ν_n is the same on both sides then $N_n = 0$ and $q_n = 0$. The total charge of the DW is

$$q_{\text{DW}} = \sum_{n=1}^{L_y/2} q_n. \quad (H12)$$

(b) When L_y is odd the Hamiltonian can be decomposed into $\lfloor L_y/2 \rfloor$ 4×4 blocks obeying the same symmorphic chiral symmetries. Each of these modes carries charges $q_n = -1, 0, 1$ $(n = 1, \ldots \lfloor L_y/2 \rfloor)$. Additionally there exists one transverse mode $n = 0$ which is similar as the one studied in the case of single-mode SSG chain. Thus, this transverse mode carries a charge $q_0 = (\pm 1 - \delta)/2$ in the case of solitons and $q_0 = (\pm 1 + \delta)/2$ in the case of antisolitons. The total charge of the DW is

$$q_{\text{DW}} = \sum_{n=0}^{\lfloor L_y/2 \rfloor} q_n. \quad (H13)$$

[1] W. P. Su, J. R. Schrieffer, and A. J. Heeger, Solitons in Polyacetylene, Phys. Rev. Lett. **42**, 1698 (1979).

[2] W. P. Su, J. R. Schrieffer, and A. J. Heeger, Soliton excitations in polyacetylene, Phys. Rev. B **22**, 2099 (1980).

[3] A. J. Heeger, S. Kivelson, J. R. Schrieffer, and W. P. Su, Solitons in conducting polymers, Rev. Mod. Phys. **60**, 781 (1988).

[4] M. Z. Hasan and C. L. Kane, Colloquium: Topological insulators, Rev. Mod. Phys. **82**, 3045 (2010).

[5] C.-K. Chiu, J. C. Y. Teo, A. P. Schnyder, and S. Ryu, Classification of topological quantum matter with symmetries, Rev. Mod. Phys. **88**, 035005 (2016).

[6] R. Jackiw and C. Rebbi, Solitons with fermion number 1/2, Phys. Rev. D **13**, 3398 (1976).

[7] E. Khalaf, W. A. Benalcazar, T. L. Hughes, and R. Queiroz, Boundary-obstructed topological phases, arXiv:1908.00011; D. V. Else, H. C. Po, and H. Watanabe, Fragile topological phases in interacting systems, Phys. Rev. B **99**, 125122 (2019).

[8] M. J. Rice and E. J. Mele, Elementary Excitations of a Linearly Conjugated Diatomic Polymer, Phys. Rev. Lett. **49**, 1455 (1982).

[9] S. A. Brazovskii, Self-localized excitations in the Peierls-Fröhlich state, Zh. Eksp. Teor. Fiz. **78**, 677 (1980) [Sov. Phys. JETP **51**, 342 (1980)].

[10] R. Jackiw and G. Semenoff, Continuum Quantum Field Theory for a Linearly Conjugated Diatomic Polymer with Fermion Fractionization, Phys. Rev. Lett. **50**, 439 (1983).

[11] D. Vanderbilt and R. D. King-Smith, Electric polarization as a bulk quantity and its relation to surface charge, Phys. Rev. B **48**, 4442 (1993).

[12] S. Onoda, S. Murakami, and N. Nagaosa, Topological Nature of Polarization and Charge Pumping in Ferroelectrics, Phys. Rev. Lett. **93**, 167602 (2004).

[13] Z. G. Soos and A. Painelli, Metastable domains and potential energy surfaces in organic charge-transfer salts with neutral-ionic phase transitions, Phys. Rev. B **75**, 155119 (2007).

[14] M. Tsuchiizu, H. Yoshioka, and H. Seo, Phase competition, solitons, and domain walls in neutral–ionic transition systems, J. Phys. Soc. Jpn. **85**, 104705 (2016).

[15] J. Goldstone and F. Wilczek, Fractional Quantum Numbers on Solitons, Phys. Rev. Lett. **47**, 986 (1981).

[16] T. Kitagawa, M. A. Broome, A. Fedrizzi, M. S. Rudner, E. Berg, I. Kassal, A. Aspuru-Guzik, E. Demler, and A. G. White, Observation of topologically protected bound states in photonic quantum walks, Nat. Commun. **3**, 882 (2012).

[17] J. Arkinstall, M. H. Teimourpour, L. Feng, R. El-Ganainy, and H. Schomerus, Topological tight-binding models from nontrivial square roots, Phys. Rev. B **95**, 165109 (2017).

[18] M. Atala, M. Aidelsburger, J. T. Barreiro, D. Abanin, T. Kitagawa, E. Demler, and I. Bloch, Direct measurement of the Zak phase in topological Bloch bands, Nat. Phys. **9**, 795 (2013).

[19] L. Wang, M. Troyer, and X. Dai, Topological Charge Pumping in a One-Dimensional Optical Lattice, Phys. Rev. Lett. **111**, 026802 (2013).

[20] M. Lohse, C. Schweizer, O. Zilberberg, M. Aidelsburger, and I. Bloch, A Thouless quantum pump with ultracold bosonic atoms in an optical superlattice, Nat. Phys. **12**, 350 (2016).

[21] S. Nakajima, T. Tomita, S. Taie, T. Ichinose, H. Ozawa, L. Wang, M. Troyer, and Y. Takahashi, Topological Thouless pumping of ultracold fermions, Nat. Phys. **12**, 296 (2016).

[22] M. Leder, C. Grossert, L. Sitta, M. Genske, A. Rosch, and M. Weitz, Real-space imaging of a topologically protected edge state with ultracold atoms in an amplitude-chirped optical lattice, Nat. Commun. **7**, 13112 (2016).

[23] E. J. Meier, F. A. An, and B. Gadway, Observation of the topological soliton state in the Su-Schrieffer-Heeger model, Nat. Commun. **7**, 13986 (2016).

[24] L. Yan and P. Liljeroth, Engineered electronic states in atomically precise nanostructures: Artificial lattices and graphene nanoribbons, Adv. Phys. X **4**, 1651672 (2019).

[25] J.-H. Park, G. Yang, J. Klinovaja, P. Stano, and D. Loss, Fractional boundary charges in quantum dot arrays with density modulation, Phys. Rev. B **94**, 075416 (2016).

[26] R. Drost, T. Ojanen, A. Harju, and P. Liljeroth, Topological states in engineered atomic lattices, Nat. Phys. **13**, 668 (2017).

[27] M. Nurul Huda, S. Kezilebieke, T. Ojanen, R. Drost, and P. Liljeroth, Tuneable topological domain wall states in engineered atomic chains, npj Quantum Mater. **5**, 17 (2020).

[28] D. J. Rizzo, G. Veber, T. Cao, C. Bronner, T. Chen, F. Zhao, H. Rodriguez, S. G. Louie, M. F. Crommie, and F. R. Fischer, Topological band engineering of graphene nanoribbons, Nature (London) **560**, 204 (2018).

[29] O. Gröning, S. Wang, X. Yao, C. A. Pignedoli, G. Borin Barin, C. Daniels, A. Cupo, V. Meunier, X. Feng, A. Narita, K. Müllen, P. Ruffieux, and R. Fasel, Engineering of robust topological quantum phases in graphene nanoribbons, Nature (London) **560**, 209 (2018).

[30] M. Weber, F. P. Toldin, and M. Hohenadler, Competing orders and unconventional criticality in the Su-Schrieffer-Heeger model, Phys. Rev. Research **2**, 023013 (2020).

[31] G. Pupillo, A. Griessner, A. Micheli, M. Ortner, D.-W. Wang, and P. Zoller, Cold Atoms and Molecules in Self-Assembled Dipolar Lattices, Phys. Rev. Lett. **100**, 050402 (2008).

[32] F. Herrera and R. V. Krems, Tunable Holstein model with cold polar molecules, Phys. Rev. A **84**, 051401(R) (2011).

[33] P. Hague and C. MacCormick, Quantum simulation of electron-phonon interactions in strongly deformable materials, New J. Phys. **14**, 033019 (2012).

[34] A. Mezzacapo, J. Casanova, L. Lamata, and E. Solano, Digital Quantum Simulation of the Holstein Model in Trapped Ions, Phys. Rev. Lett. **109**, 200501 (2012).

[35] U. Bissbort, D. Cocks, A. Negretti, Z. Idziaszek, T. Calarco, F. Schmidt-Kaler, W. Hofstetter, and R. Gerritsma, Emulating Solid-State Physics with a Hybrid System of Ultracold Ions and Atoms, Phys. Rev. Lett. **111**, 080501 (2013).

[36] M. Płodzień, T. Sowiński, and S. Kokkelmans, Simulating polaron biophysics with Rydberg atoms, Sci. Rep. **8**, 9247 (2018).

[37] K. Shiozaki, M. Sato, and K. Gomi, Z_2 topology in nonsymmorphic crystalline insulators: Möbius twist in surface states, Phys. Rev. B **91**, 155120 (2015).

[38] L. Fu and C. L. Kane, Topological insulators with inversion symmetry, Phys. Rev. B **76**, 045302 (2007).

[39] W. Brzezicki, J. Dziarmaga, and A. M. Oleś, Topological Order in an Entangled $SU(2) \otimes XY$ Spin-Orbital Ring, Phys. Rev. Lett. **112**, 117204 (2014).

[40] A. Topp, R. Queiroz, A. Grüneis, L. Müchler, A. W. Rost, A. Varykhalov, D. Marchenko, M. Krivenkov, F. Rodolakis, J. L. McChesney, B. V. Lotsch, L. M. Schoop, and C. R. Ast, Surface Floating 2D Bands in Layered Nonsymmorphic Semimetals: ZrSiS and Related Compounds, Phys. Rev. X **7**, 041073 (2017).

[41] W. Brzezicki, M. M. Wysokiński, and T. Hyart, Topological properties of multilayers and surface steps in the SnTe material class, Phys. Rev. B **100**, 121107(R) (2019).

[42] G. P. Mazur, K. Dybko, A. Szczerbakow, J. Z. Domagala, A. Kazakov, M. Zgirski, E. Lusakowska, S. Kret, J. Korczak, T. Story, M. Sawicki, and T. Dietl, Experimental search for the origin of low-energy modes in topological materials, Phys. Rev. B **100**, 041408(R) (2019).

[43] C.-Y. Hou, C. Chamon, and C. Mudry, Electron Fractionalization in Two-Dimensional Graphenelike Structures, Phys. Rev. Lett. **98**, 186809 (2007).